

ORIGINAL RESEARCH

Biomechanical Stress Profiling of Coronary Atherosclerosis

Identifying a Multifactorial Metric to Evaluate Plaque Rupture Risk

Pallavi Doradla, PhD,^{a,*} Kenichiro Otsuka, MD, PhD,^a Abhijay Nadkarni,^a Martin Villiger, PhD,^a Antonios Karanasos, MD, PhD,^b Laurens J.C. van Zandvoort, MD,^b Jouke Dijkstra, PhD,^c Felix Zijlstra, MD, PhD,^b Gijs van Soest, PhD,^b Joost Daemen, MD, PhD,^b Evelyn Regar, MD, PhD,^b Brett E. Bouma, PhD,^{a,d} Seemantini K. Nadkarni, PhD^{a,*}

ABSTRACT

OBJECTIVES The purpose of this study was to derive a biomechanical stress metric that was based on the multifactorial assessment of coronary plaque morphology, likely related to the propensity of plaque rupture in patients.

BACKGROUND Plaque rupture, the most frequent cause of coronary thrombosis, occurs at locations of elevated tensile stress in necrotic core fibroatheromas (NCFAs). Finite element modeling (FEM), typically used to calculate tensile stress, is computationally intensive and impractical as a clinical tool for locating rupture-prone plaques. This study derived a multifactorial stress equation (MSE) that accurately computes peak stress in NCFAs by combining the influence of several morphological parameters.

METHODS Intravascular ultrasound and optical frequency domain imaging were conducted in 30 patients, and plaque morphological parameters were defined in 61 NCFAs. Multivariate regression analysis was applied to derive the MSE and compute a peak stress metric (PSM) that was based on the analysis of plaque morphological parameters. The accuracy of the MSE was determined by comparing PSM with FEM-derived peak stress values. The ability of the PSM in locating plaque rupture sites was tested in 3 additional patients.

RESULTS The following parameters were found to be independently associated with peak stress: fibrous cap thickness ($p < 0.0001$), necrotic core angle ($p = 0.024$), necrotic core thickness ($p < 0.0001$), lumen area ($p < 0.0001$), necrotic core including calcium areas ($p = 0.017$), and plaque area ($p = 0.003$). The PSM showed excellent correlation ($R = 0.85$; $p < 0.0001$) with FEM-derived peak stress, thus confirming the accuracy of the MSE. In only 56% ($n = 34$) of plaques, the thinnest fibrous cap thickness was a determining parameter in identifying the cross section with highest PSM. In coronary segments with plaque ruptures, the MSE precisely located the rupture site.

CONCLUSIONS The MSE shows potential to calculate the PSM in coronary lesions rapidly. However, further studies are warranted to investigate the use of biomechanical stress profiling for the prognostic evaluation of patients with atherosclerosis. (J Am Coll Cardiol Img 2019;■:■-■) © 2019 by the American College of Cardiology Foundation.

From the ^aWellman Center for Photomedicine, Massachusetts General Hospital, Harvard Medical School, Boston, Massachusetts; ^bDepartment of Interventional Cardiology, Thorax Center, Erasmus Medical Center, Rotterdam, the Netherlands; ^cDepartment of Radiology, Leiden University Medical Center, Leiden, the Netherlands; and the ^dHarvard-Massachusetts Institute of Technology, Program in Health Sciences and Technology, Cambridge, Massachusetts. This work was supported by the National Institutes of Health contract NIH R01HL119065 and in part by Terumo Corporation. Dr. Villiger's institution has patent licensing arrangements with Terumo Corporation, and he has the right to receive royalties as part of this patent licensing arrangements. Dr. van Soest's institution has a patent licensing agreement with Terumo Corporation, and he has the right to receive royalties as part of that agreement. Dr. Bouma's institutions have patent licensing arrangements with Terumo Corporation, and he has the right to receive royalties as part of the arrangements; and he has received grant NIH P41EB015903. Dr. S.K. Nadkarni is on the

ABBREVIATIONS AND ACRONYMS

ACS = acute coronary syndrome

CT = computed tomography

CTA = computed tomography angiography

FEM = finite element modeling

IVUS = intravascular ultrasound

MSE = multifactorial stress equation

NC = necrotic core

NCFA = necrotic core fibroatheroma

OFDI = optical frequency domain imaging

PCI = percutaneous coronary intervention

PSM = peak stress metric

TCFA = thin-cap fibroatheroma

Ruptured thin-cap fibroatheromas (TCFAs), frequently implicated at the site of culprit coronary thrombi, are hallmarked by the presence of a thin, inflamed fibrous cap overlying a large necrotic lipid core (1,2). Motivated by the need to identify rupture-prone plaques prospectively in patients, a number of intravascular modalities, including optical frequency domain imaging (OFDI), virtual histology, intravascular ultrasound (IVUS), and near-infrared spectroscopy, have been investigated to detect TCFAs (3,4). A critical challenge is that TCFAs with similar morphological features do not all possess an equal likelihood of rupture. In 70% of patients with acute coronary syndrome (ACS), multiple nondisrupted TCFAs are found remote from the culprit site and in nonculprit arteries (5,6). Moreover, 20% of plaque ruptures are observed in necrotic core (NC)

lesions with thicker fibrous caps (>100 μ m), intraplaque hemorrhage, or calcifications (5-7). These findings call into question the effectiveness of an imaging paradigm that relies entirely on detecting TCFA features and highlight the need to augment morphological findings with critical biomechanical metrics to evaluate the risk of plaque rupture accurately.

Finite element modeling (FEM) is a widely accepted computational tool for biomechanical profiling of coronary plaques. In FEM, plaque contours are determined using idealized models (8,9), histology cross sections (10,11), or imaging tools such as virtual histology, IVUS, or computed tomography (CT) (12-14). The contours are discretized into meshes, and tensile stress is mathematically derived in response to physiological pressure and information on the material properties of the constituent tissues (8,12). Several FEM studies have underscored the importance of local maximum (peak) tensile stress in the fibrous cap and indicated that peak stress is profoundly related to the propensity of plaque rupture and ensuing risk of acute coronary events (12-14). Various morphological factors, including fibrous cap thickness (8,11), NC size (11,12,14), plaque burden (13), stenosis severity (8), and presence of calcifications

(13), have been shown to influence peak stress. Clinical studies suggest that the measurement of peak stress may improve the prediction of future major adverse cardiovascular events, thus highlighting the clinical need for prospectively quantifying biomechanical stress in coronary plaques (13,15). However, despite the demonstrated relevance and clinical need for measuring plaque tensile stress, the computational complexity and long processing times render the FEM approach impractical as a routine clinical tool for biomechanical stress profiling of coronary plaques.

In this study, we introduce a novel approach using a straightforward multifactorial stress equation (MSE), which may circumvent the need for FEM by estimating peak stress in necrotic core fibroatheromas (NCFAs) directly from 6 independent morphometric measurements of plaque geometry. To improve the precision of quantifying peak stress, the MSE uses a dual-modality OFDI-IVUS approach to obtain plaque morphology. Through studies conducted in 33 patients, we demonstrate that the new MSE can accurately estimate peak stress to potentially locate rupture-prone plaques in patients.

METHODS

STUDY GROUP. This study details a retrospective analysis of an investigational study that included 33 patients with ACS ($n = 13$) and stable angina pectoris ($n = 20$) who underwent imaging using IVUS according to standard of care, followed by OFDI imaging between August 2008 and July 2015 at the Thorax Center, Erasmus Medical Center, Rotterdam, the Netherlands (Supplemental Table 1). The Ethics Committee at Erasmus Medical Center approved the protocol (Ref: NL 22249.078.08). Each patient gave written informed consent before enrollment. All procedures were performed in accordance with local and federal regulations and the Declaration of Helsinki.

OFDI AND IVUS IMAGING. OFDI and IVUS imaging were performed following diagnostic coronary angiography in 33 patients (10 before percutaneous coronary intervention [PCI], 8 after PCI, and 15 both before and after PCI). Gray scale IVUS (3.2-F, 30 MHz, Boston Scientific, Marlborough, Massachusetts;

Board of Directors of Coalesenz; and has received grant support from the National Institutes of Health for retrospective analysis of optical frequency domain imaging and intravascular ultrasound images in this study. All other authors have reported that they have no relationships relevant to the contents of this paper to disclose. *Dr. Doradla is the first author of this manuscript and Dr. Nakami is the Principal Investigator of the lab. Gregg Stone, MD, served as Guest Editor for this article.

Manuscript received November 8, 2018; revised manuscript received December 31, 2018, accepted January 2, 2019.

100- μ m axial resolution) was performed with 0.5 mm/s pullback speed at 10 frames/s. Separate OFDI pullbacks were performed following IVUS through the same guide wire and using an imaging protocol that has been well established (16). Using 2.6-F catheters (Terumo Fast View, Terumo Corporation, Somerset, New Jersey), OFDI (console built at Massachusetts General Hospital, Boston, Massachusetts; 1300-nm center wavelength, 9.4- μ m axial resolution) was performed at 20 mm/s pullback speed with an imaging rate of 100 frames/s during injection of nonionic contrast solution at 1 to 3 ml/s (17).

OFDI-IVUS IMAGE CO-REGISTRATION. OFDI and IVUS image co-registration was performed using previously established criteria for plaque identification (18) with ImageJ (National Institutes of Health, Bethesda, Maryland). Image cross sections with stent struts, side branches spanning beyond the field of view, or visible thrombi were excluded from the analysis because these features obstructed the accurate determination of luminal geometry. IVUS datasets were co-registered with OFDI pullbacks with the aid of landmarks, such as side branches, presence of calcifications, lumen shape, plaque shape, and the relative distance from such landmarks and structures. From OFDI images, we identified all NCFAs defined as plaques with a high-intensity fibrous cap overlying an NC with low-intensity, diffused signal, with a lipid arc $>90^\circ$. A total of 61 nonruptured NCFAs were identified in 39 coronary arteries of 30 patients. Co-registered OFDI-IVUS image pairs at the location of the thinnest fibrous cap in all 61 NCFAs were selected for analysis using FEM (detailed later). In addition, to investigate the influence of plaque morphological parameters, OFDI-IVUS image pairs were further selected for analysis at 1-mm increments over the entire length for each NCFAs. Thus, a total of 195 co-registered OFDI-IVUS image pairs from 61 nonruptured NCFAs were analyzed. In 3 additional patients, ruptured NCFAs were observed at the sites of culprit coronary thrombosis; these patients' datasets were used to test the use of the MSE for localizing plaque ruptures as detailed later.

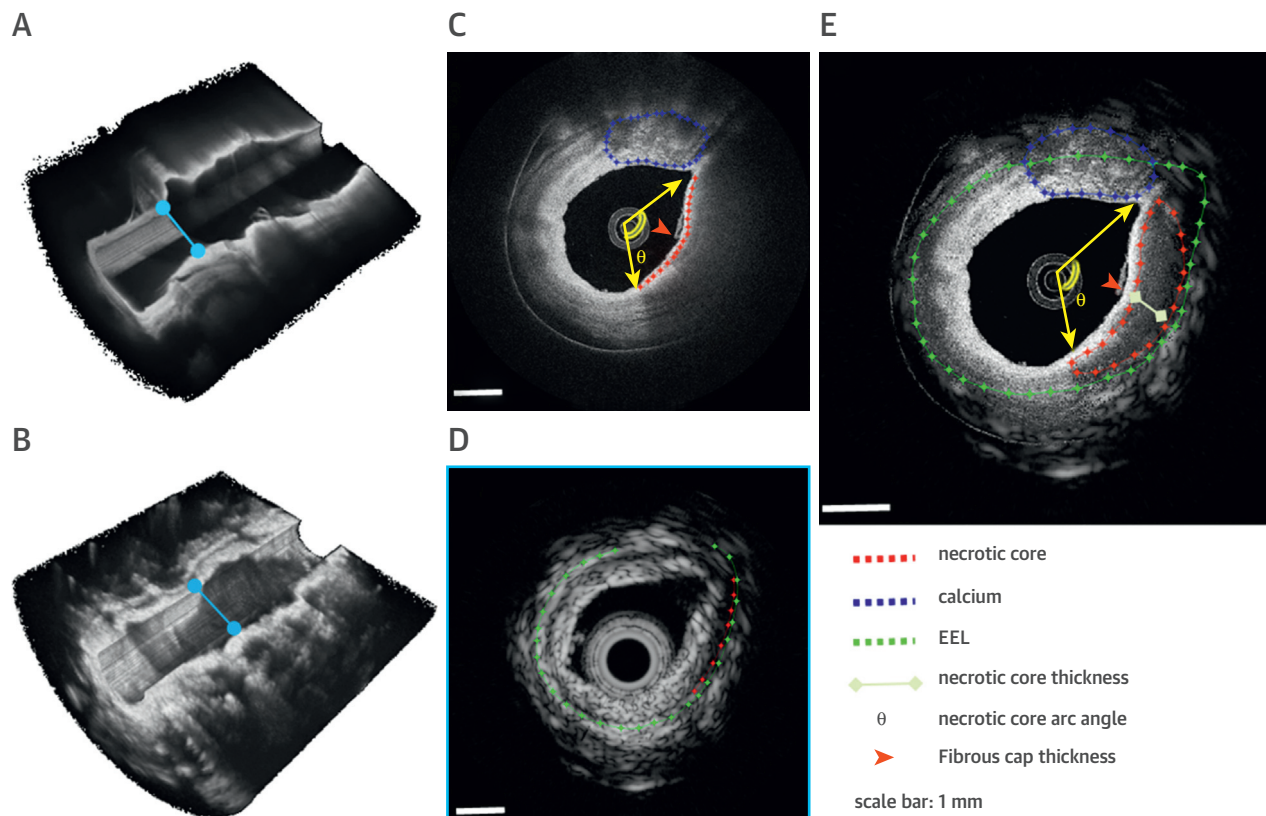
DEFINITION AND MEASUREMENT OF PLAQUE PARAMETERS. In all 33 patients, NCFAs morphological parameters were quantified following manual segmentation of the lumen, fibrous cap and calcium contours from OFDI images, and the NC and external elastic lamina (EEL) contours from composite OFDI-IVUS images (Figures 1A to 1E) by using QCU-CMS software (Leiden University Medical Center, Leiden, the Netherlands). All parameters were calculated as an average of measurements performed in triplicate.

From OFDI images, fibrous cap thickness (FC_{thick} = minimum radial thickness), NC arc angle (NC_{arc} = maximum circumferential arc), calcium thickness (Cal_{thick}), and calcium-lumen distance (Cal_{depth}) were measured (Figure 1C). From the composite OFDI-IVUS images, plaque thickness (Plq_{thick} = distance between lumen and EEL), NC thickness (NC_{thick} = NC thickness at the location of thinnest cap region), lumen (CSA_{lumen}), necrotic core (NC_{area}), and calcium areas (Cal_{area}) were measured (Figure 1E). Tot_{area} was defined as the area of the coronary cross section encompassed by the EEL, Plq_{area} was measured by excluding CSA_{lumen} from the Tot_{area} ($Plq_{area} = Tot_{area} - CSA_{lumen}$), and percent area stenosis (%AS) was derived from OFDI by: $(1 - CSA_{lumen} / [RefLu_{area}]) \cdot 100\%$.

FINITE ELEMENT MODELING. To derive the MSE, we first investigated the relationships between individual plaque parameters and peak stress values in 61 nonruptured NCFAs cross sections selected at the location of the thinnest fibrous cap. FEM was used to calculate reference peak stress values because it is the most widely used and validated approach for biomechanical analysis (8-14) (see Supplemental Appendix for details).

Material and model properties. Plaque geometry was reconstructed from the segmented contours by using a simple MATLAB (MathWorks, Natick, Massachusetts) script (Figures 2A to 2E) and exported to ABAQUS software (version 6.14, Dassault Systèmes [3DS], Boston, Massachusetts) to perform FEM. An anisotropic, linear-elastic, quasi-incompressible material model was used to conduct FEM, similar to other published reports (8,12). The material properties of the plaque constituents were obtained from published reports (8,15,19) (Supplemental Table 2).

Mesh generation and modal solution. The segmented plaque geometries were meshed with 2-dimensional, 6-node triangular and 8-node quadrilateral isoparametric elements. Appropriate boundary conditions and wall thickness of 300 μ m were used to suppress the rigid body motion and radial overstretching of the artery, respectively. Static intraluminal pressure of 13.33 kPa was applied as the loading condition to mimic physiological pressure. The distribution of tensile stress was computed within each element, and the average stress of neighboring elements was calculated to obtain the tensile stress at each node. The tensile stress distribution was similarly calculated for all nodes within the coronary cross section, and the location of the maximum tensile stress (peak stress) was noted (Figure 2D).

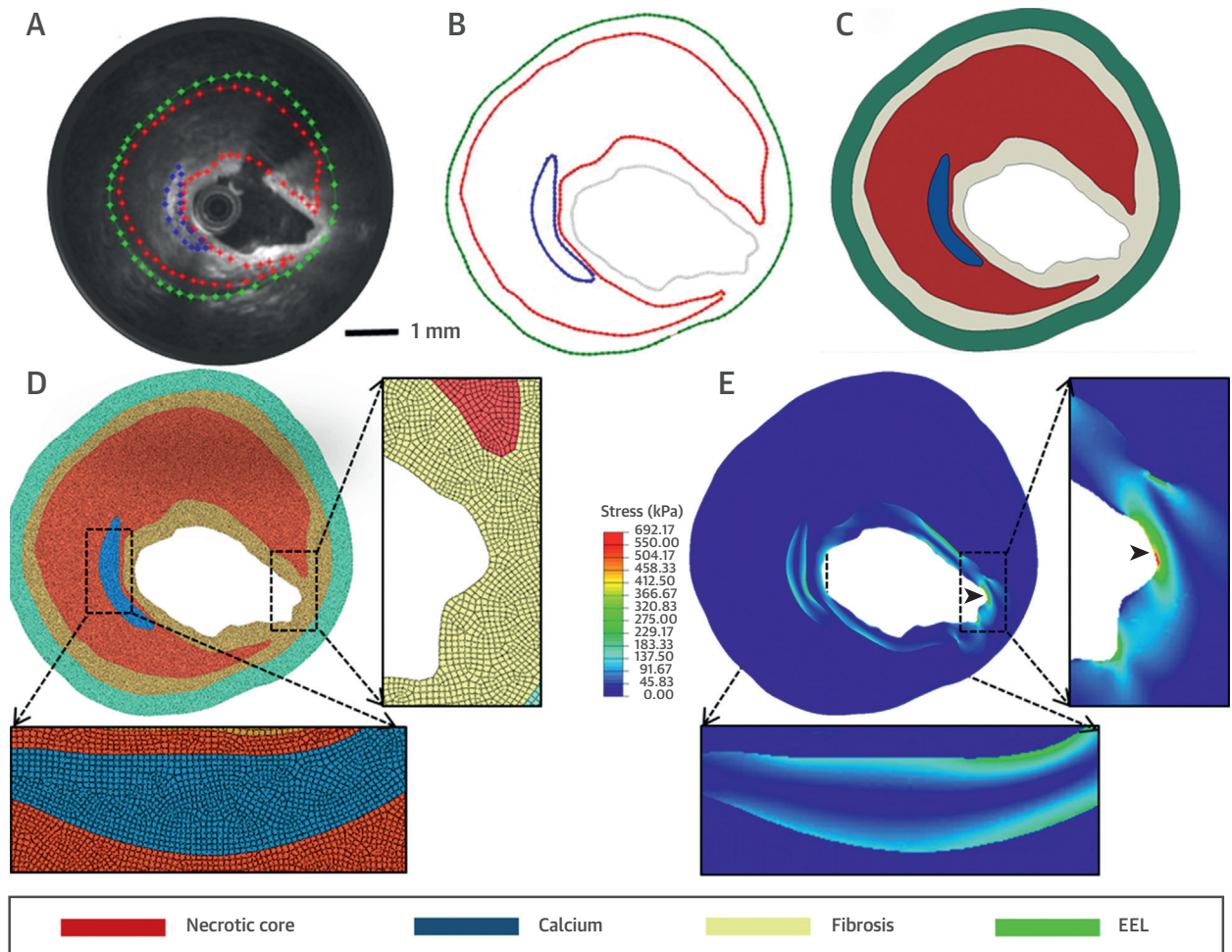
FIGURE 1 Intracoronary OFDI and IVUS Assessment of Plaque Geometry in Patients

Shown are 2-cm-long pullbacks of (A) optical frequency domain imaging (OFDI) and (B) intravascular ultrasound (IVUS) through a coronary artery. The corresponding 2-dimensional cross-sectional images of a typical coronary plaque with lipid pool are shown at the location of the blue line. (C) Optical frequency domain imaging identifies a thin fibrous cap (red arrowhead) over a lipid pool (yellow arc). (D) Intravascular ultrasound detects the external elastic membrane (green line). (E) Combined plaque boundaries obtained from superposed optical frequency domain imaging and intravascular ultrasound images. EEL = external elastic lamina.

STATISTICAL ANALYSIS. Univariate linear regression analysis was used to analyze the extent of correlation between each of the 13 plaque parameters and the FEM-derived peak stress. Then, a stepwise multivariate regression model (SPSS version 24.0.0, IBM Corp., Armonk, New York) was used to determine the interdependencies among plaque variables and to identify the most influential parameters. In some cases, multiple NCFAs were identified in the same patient; therefore, the generalized estimating equation was used to account for inpatient dependencies. In all cases, $p < 0.05$ was considered statistically significant. The principal plaque parameters that significantly influenced the peak stress were used to derive the MSE. The accuracy of the MSE was evaluated by comparing the MSE-calculated peak stress metric (PSM) with the FEM-measured peak stress values using the leave-1-out cross-validation method.

RESULTS

PEAK STRESS IN NCFAs LESIONS. The FEM-derived peak stress in 61 NCFAs ranged from 108.8 to 1048.0 kPa and was located at the shoulder of the NC ($n = 32$), summit of the NC ($n = 11$), boundary between calcium and lipid or at the edge of calcific nodule ($n = 10$), and along the longest diameter (major axis) of the plaque ($n = 8$) of NCFAs. Figures 3A1 to 3A5 to 3C1 to 3C5 illustrate 5 multifarious NCFAs with 96 to 424 μm FC_{thick} , 602 to 993 μm NC_{thick} , 98 to 302° NC_{arc} , and with or without calcium inclusions. The OFDI images, corresponding OFDI-IVUS composite images with segmented contours, and reconstructed plaque geometries, with the tensile stress distributions, are displayed. Similar to other studies (13), we observed that the location of peak stress was limited to within the superficial 500 μm of the plaque. Similar to prior FEM studies (8,11,12,19), we observed that

FIGURE 2 FEM to Measure Coronary Tensile Stress Distribution

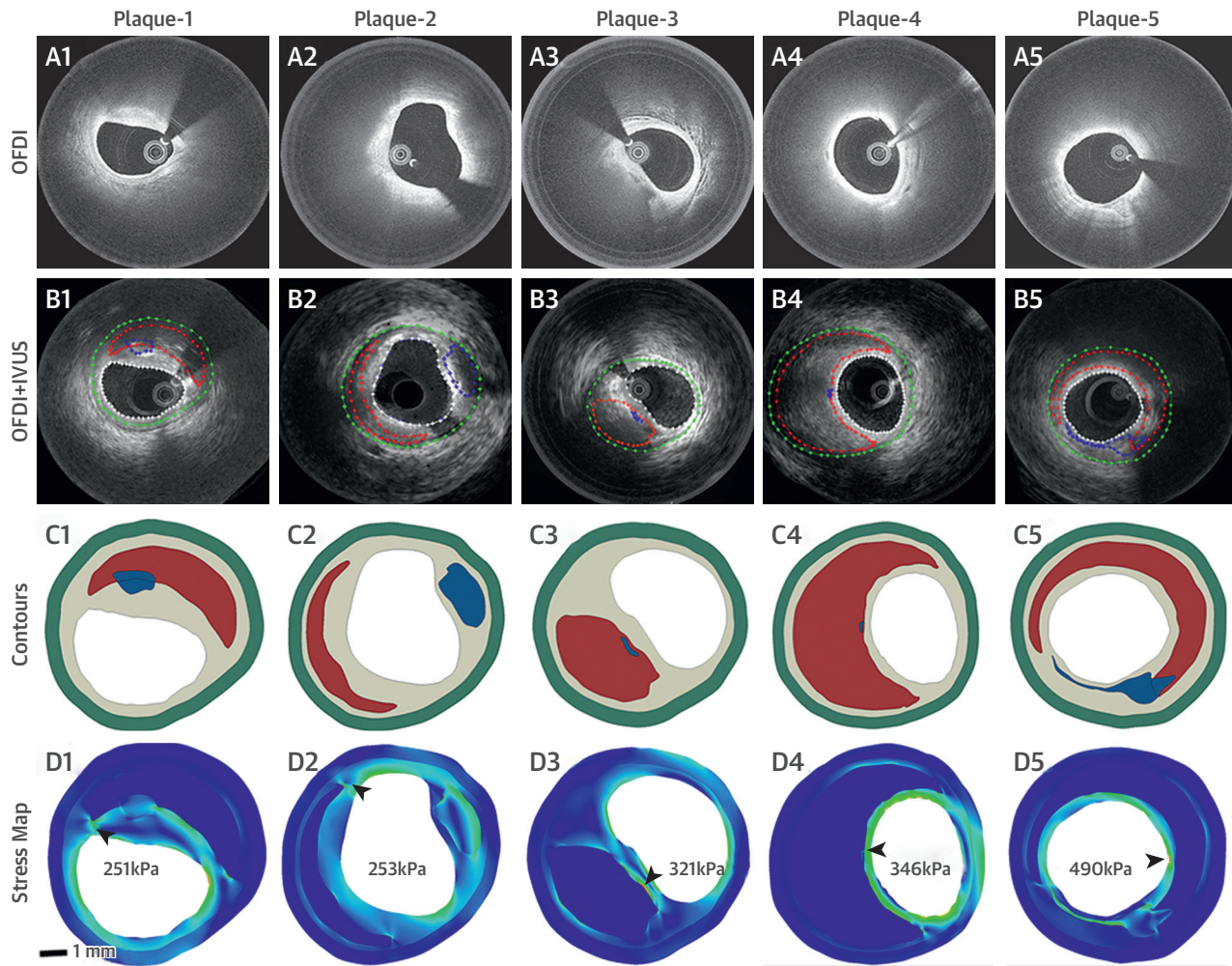
(A) Optical frequency domain imaging and intravascular ultrasound overlay of a necrotic core fibroatheroma (NCFA) cross section showing plaque contours.

(B) Extracted contours from (A). (C) Plaque geometry reconstructed from the contours. (D) Finite element quadrangular mesh with inset showing magnified image of fine mesh. (E) Tensile stress distribution calculated using finite element modeling (FEM) analysis. **Arrowhead** = peak stress location. EEL = external elastic lamina.

peak stress varied inversely with FC_{thick} ; high peak stress values were measured in NCFAs with thinner fibrous caps (Figure 3D3 to 3D5). Furthermore, thicker NCs with large NC_{arc} elicited high peak stress. We also observed that the presence, location, and thickness of calcium modulated peak stress. Furthermore, the interactions among multiple morphometric plaque parameters greatly influenced the magnitude and location of peak stress. For instance, because of the presence of thin calcium near the lumen, an elevated peak stress of 321 kPa (Figure 3D3) was measured in the NCFA with the smallest arc angle (98°), and a peak stress of 346 kPa (Figure 3D4) was measured in the NCFA with a relatively thicker fibrous cap ($116 \mu m$). A high peak stress of 490 kPa was observed at the

summit of the plaque with a thick NC and large arc angle, as seen in Figure 3D4.

CORRELATION BETWEEN PLAQUE PARAMETERS AND FEM-DERIVED PEAK STRESS. The correlation between FEM-derived peak stress and the following 13 plaque parameters was investigated: FC_{thick} , NC_{thick} , NC_{arc} , CSA_{lumen} , $NCCal_{area}$, Plq_{area} , Cal_{thick} , Cal_{depth} , Plq_{thick} , NC_{area} , Cal_{area} , Tot_{area} , and $\%AS$. The mean \pm SD for each plaque parameter is shown in Table 1. First, by univariate linear regression analysis, we identified FC_{thick} , NC_{arc} , NC_{thick} , Plq_{thick} , CSA_{lumen} , $NCCal_{area}$, Plq_{area} , and Tot_{area} as the 8 parameters that significantly correlated with FEM-derived peak stress (Figures 4A to 4H). Although 7 plaque parameters showed a linear trend, a nonlinear relationship was

FIGURE 3 Multifarious Coronary NCFA Geometries in Patients

(A1 to A5) optical frequency domain imaging (OFDI), (B1 to B5) combined optical frequency domain imaging and intravascular ultrasound (IVUS) with plaque contours, (C1 to C5) plaque geometry reconstructed from the contours, and (D1 to D5) maps of tensile stress distribution calculated by finite element modeling. A large range of peak stress values (**black arrowheads**) is observed in the 5 necrotic core fibroatheromas (NCFAs) influenced by plaque geometry.

observed between FEM-derived peak stress and FC_{thick} , and the best fit was obtained using power law (8,11,12).

MOST INFLUENTIAL PARAMETERS AND THE MSE.

We used stepwise multivariate regression analysis to identify the most influential plaque parameters and exclude redundant variables (Table 2). We observed that both plaque thickness and total area were excluded by the multivariate stepwise regression analysis from the predictor list. This was because plaque thickness was found to be collinear with the plaque area. Total area was found to be redundant because it is the sum of lumen and plaque areas, and it was excluded from the final MSE model. Thus, only

the following 6 parameters (out of the initial 13) independently influenced peak stress and were used to develop the MSE: FC_{thick} ($p < 0.0001$), NC_{arc} ($p = 0.024$), NC_{thick} ($p < 0.0001$), CSA_{lumen} ($p < 0.0001$), $NCCal_{area}$ ($p = 0.017$), and Plq_{area} ($p = 0.003$). Consequently, using the regression coefficients (B_i) (Table 2), the MSE was developed by combining the cumulative interactions of 6 plaque parameters to compute the PSM as follows:.

$$PSM = -0.598 - 146.07 \times \log(FC_{thick}) + 0.608 \times NC_{arc} + 223.41 \times NC_{thick} + 22.56 \times CSA_{lumen} + 33.58 \times (NCCal_{area}) - 29.67 \times Plq_{area} \quad (\text{Equation 1})$$

MSE VERSUS FEM-DERIVED PEAK STRESS. To evaluate the accuracy of the MSE in estimating peak stress directly from plaque parameters, the MSE-calculated PSM was compared against FEM-derived peak stress using the leave-1-out cross-validation method. Excellent correlation ($R = 0.85$; $p < 0.0001$) was observed (Figure 5A) between PSM and FEM-derived peak stress in 61 NCFA cross sections, thus confirming the accuracy of the MSE. Figure 5B shows the results of the Bland-Altman analysis with a negligible bias of 0.27 kPa in the MSE estimation of peak stress. These results demonstrate that the absolute values of PSM calculated by MSE are similar to those computed by FEM.

INFLUENCE OF PLAQUE PARAMETERS ON MSE-DERIVED PEAK STRESS. In 61 nonruptured NCFAs, 195 image pairs selected at 1-mm increments along the length of the NCFA were analyzed using the MSE (Equation 1) to identify cross sections with the highest PSM value. We observed that cross sections with the highest PSM along the NCFA length coincided with the locations of the thinnest fibrous caps in 56% ($n = 34$) of plaques, whereas in 44% ($n = 27$) of plaques, the highest PSM occurred at cross sections distinct from that of the thinnest fibrous cap. Furthermore, the FC_{thick} was the sole determining factor for the highest PSM in only 7% of analyzed sections, and a combination of parameters including the FC_{thick} influenced the highest PSM in 49% of cases (Supplemental Figure 2). In the remaining 44% of plaques in which smallest FC_{thick} was not a determining factor, the highest PSM was found at cross-sectional frames with the largest NC_{thick} (7%; $n = 4$), NC_{arc} (3%; $n = 2$), Plq_{area} (3%; $n = 2$), $NCCal_{area}$ (2%; $n = 1$), smallest CSA_{lumen} (5%; $n = 3$), and a combination of other plaque parameters (24%; $n = 15$) that did not include the smallest FC_{thick} .

LOCATING RUPTURED NCFAs IN PATIENTS. Finally, we assessed the ability of the MSE to locate plaque ruptures in 3 patients with ruptured NCFAs observed at the sites of culprit thrombi. Figures 6A1 to 6A3 show the PSM values measured at 2 mm intervals in 3 coronary segments by retrieving the plaque parameters from each cross section and simply substituting the values into the MSE. Figures 6B1 to 6B3 display 2-dimensional cross-sectional OFDI images at 5 discrete locations along each coronary pullback; the coronary cross section with the maximum PSM is highlighted in red. Subsequently, we observed that the location of the maximum PSM with black asterisks is in close proximity to the plaque rupture sites in all 3 patients (Figures 6C1 to 6C3).

TABLE 1 The Correlation Between FEM-Derived Peak Stress and the Imaging Plaque Parameters

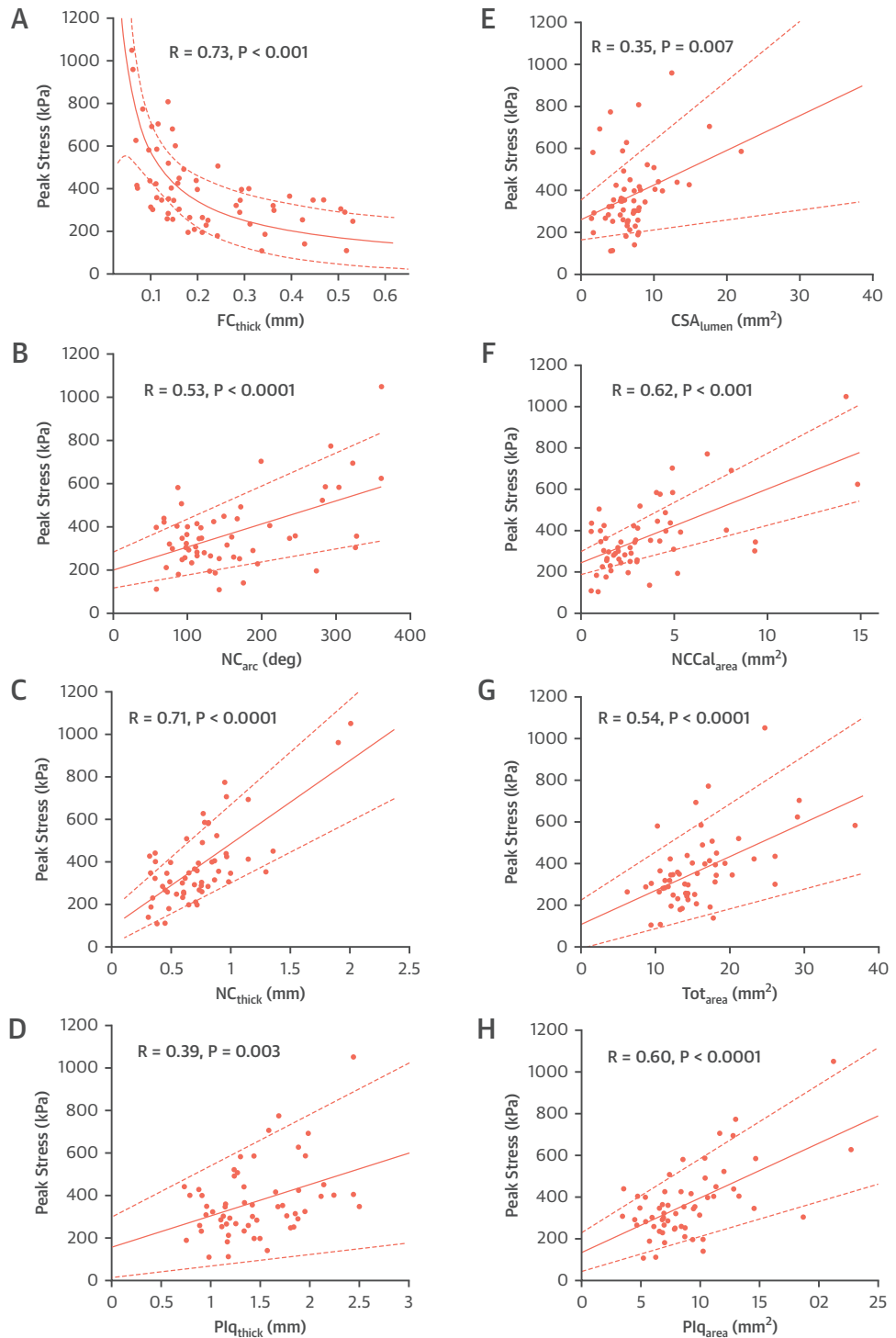
Plaque Parameter	Mean \pm SD	R	p Value
Fibrous cap thickness (FC_{thick})*	0.22 ± 0.13 mm	0.73	0.0001
Necrotic core thickness (NC_{thick})*	0.74 ± 0.33 mm	0.71	0.0001
Necrotic core arc angle (NC_{arc})*	158 ± 81	0.53	0.0001
Lumen cross-sectional area (CSA_{lumen})*	6.89 ± 3.62 mm ²	0.35	0.007
NC plus calcium area ($NCCal_{area}$)*	3.58 ± 2.89 mm ²	0.62	0.0001
Plaque area (Plq_{area})*	8.99 ± 3.79 mm ²	0.60	0.0001
Calcium thickness (Cal_{thick})	0.29 ± 0.19 mm	0.03	0.89
Calcium depth (Cal_{depth})	0.31 ± 0.17 mm	0.32	0.11
Plaque thickness (Plq_{thick})	1.45 ± 0.43 mm	0.39	0.003
Necrotic core area (NC_{area})	3.41 ± 2.87 mm ²	0.58	0.0001
Calcium area (Cal_{area})	0.60 ± 0.55 mm ²	0.32	0.09
Total area (Tot_{area})	15.9 ± 5.41 mm ²	0.54	0.0001
%Area stenosis (%AS)	$34.9 \pm 22.8\%$	0.10	0.46

*The most influential independent plaque parameters.

DISCUSSION

The tensile stress distribution in NCFAs, particularly peak stress in the fibrous cap, is a crucial predictor of plaque rupture and major adverse cardiovascular events in patients (12-14). The traditional FEM modeling approach used to compute the peak stress is mathematically complex, requires specialist operators, and takes hours to report results. In this study, we demonstrate that PSM can be readily calculated directly from morphometric measurements derived from plaque geometry. Our results show that MSE-measured PSM values are essentially identical to those obtained by FEM, thus suggesting that MSE may circumvent the need for mathematically complex and time-intensive FEM approaches to measure plaque stress. Consequently, in a pilot test in 3 patients, we showed that the locations of elevated PSM coincided with sites of ruptured plaques.

A key finding of our study is that peak stress in the fibrous cap can be directly estimated by using a closed-form equation (Equation 1). Similar to other studies (8,11,12), we demonstrated a nonlinear relationship (Figure 4A) between peak stress and FC_{thick} . Although the critical FC_{thick} of <65 μ m has been extensively reported in published reports as a major determinant of plaque vulnerability (1,18), our study demonstrated that under certain conditions, NCFAs with thicker FC_{thick} similarly exhibited elevated peak stress. We further observed that in plaques with thicker caps (>200 μ m), the peak stress is only minimally influenced by FC_{thick} , where NC_{thick} was the major determinant of PSM, whereas when FC_{thick} is reduced to less than 200 μ m, peak stress is exponentially elevated (Figure 4A). Similar to our results,

FIGURE 4 Influence of Various Plaque Parameters on Peak Stress

A strong positive correlation is observed between peak stress and **(A)** fibrous cap thickness (FC_{thick} ; $r = 0.73$; $p < 0.0001$), **(B)** NC arc angle (NC_{arc} ; $r = 0.53$; $p < 0.0001$), **(C)** NC thickness (NC_{thick} ; $r = 0.71$; $p < 0.0001$), **(D)** plaque thickness (Plq_{thick} ; $r = 0.39$; $p < 0.003$), **(E)** lumen cross-sectional area (CSA_{lumen} ; $r = 0.35$; $p = 0.007$), **(F)** NC including calcium area ($NCCal_{area}$; $r = 0.62$; $p < 0.0001$), **(G)** total area (Tot_{area} ; $r = 0.54$; $p < 0.0001$), and **(H)** plaque area (Plq_{area} ; $r = 0.60$; $p < 0.0001$).

TABLE 2 Multivariate Regression Analysis to Identify the Most Influential Plaque Parameters

Plaque Parameter	Unstandardized Coefficient		Standardized Coefficient	95% CI		Statistical Significance p Value	Collinearity Statistics	
	B	SE		Lower Bound	Upper Bound		Tolerance	VIF
(Constant)	−0.598	50.99	—	−101	99.4	0.991	—	—
FC _{thick} (mm)	−146.1	41.33	−0.210	−227	−65.0	0.000	0.513	1.948
NC _{arc} (°)	0.608	0.269	0.275	0.08	1.13	0.024	0.024	2.666
NC _{thick} (mm)	223.4	39.27	0.381	146	300	0.000	0.612	1.660
CSA _{lumen} (mm ²)	23.56	3.160	0.496	17.4	29.7	0.000	0.521	1.918
NCCa _{area} (mm ²)	33.58	14.13	0.504	5.89	61.3	0.017	0.102	9.834
Plaque _{area} (mm ²)	−29.67	9.950	−0.600	−49.2	−10.2	0.003	0.106	9.406

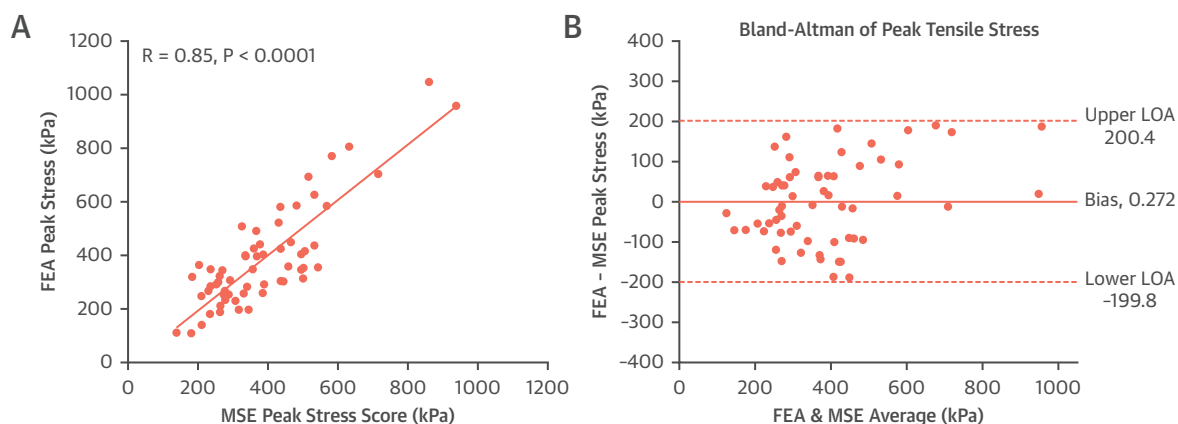
Cal = calcium; CI = confidence interval; CSA = cross-sectional area; FC = fibrous cap; NC = necrotic core; VIF = variance inflation factor.

other studies also showed that peak stress is increased with increasing luminal area, lumen eccentricity, NC thickness, NC area/NC arc, and arterial remodeling index (12,14).

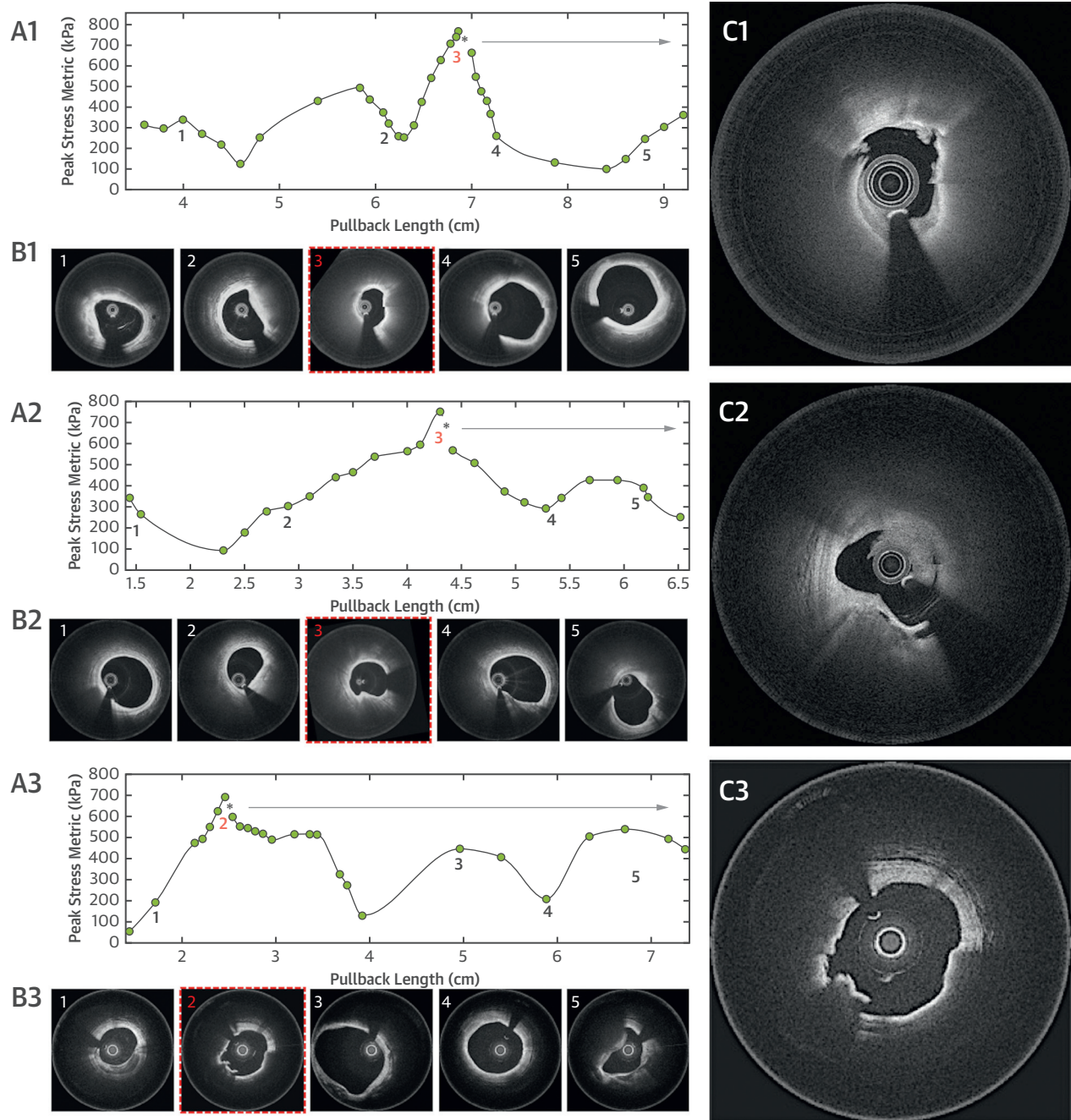
Interestingly, in our study only 56% of the plaques elicited the highest PSM at the frame with the thinnest cap location, and FC_{thick} was a sole determining factor in only 7% of plaques. In fact, prior histopathological and clinical OFDI studies have suggested that ruptured NCFAs are often observed in locations with thicker fibrous caps, calcific nodules, and increased plaque burden (5-7). Our results similarly showed that the location of the thinnest fibrous cap did not influence the highest PSM in 44% of NCFAs and that other parameters, including largest NC_{thick}, NC_{arc}, Plq_{area}, NCCa_{area}, and smallest CSA_{lumen}, were the determining factors in these cases. The results likely provide a quantitative biomechanical corroboration

for the foregoing clinical observations and provide a unique opportunity for further investigations.

Consistent with previous studies implicating the influence of calcium (20), our study demonstrated that peak stress was influenced by the presence, location, and area of calcification in the coronary cross section. When evaluated as an independent variable, Cal_{area} indicated moderate correlation with peak stress ($R = 0.35$; $p < 0.01$). However, the overlap of calcification with the NC, specifically the sum of NC_{area} and Cal_{area}, significantly influenced the peak stress ($R = 0.62$; $p < 0.0001$). These results suggest that in addition to the presence of calcification, the proximity of calcium deposits with NC is likely an important mediator of plaque rupture. We noticed that peak stress was considerably elevated when a thin calcific nodule (Cal_{thick} <200 μ m) was located in the vicinity of the lumen (Cal_{Lu}_{dist} <200 μ m).

FIGURE 5 Comparison of PSM Measured by the MSE Versus FEM

(A) Multifactorial stress equation (MSE)—measured peak stress metric (PSM) compared with finite element modeling (FEM)—derived values using leave-1-out-cross-validation shows high correlation between both methods ($R = 0.85$; $p < 0.0001$), and (B) Bland-Altman plot indicates high concordance in measurements between MSE and finite element modeling. FEA = Finite Element Analysis; LOA = Limits of Agreement.

FIGURE 6 Locating the Culprit Plaque Rupture Using the MSE Tool

(A1 to A3) Peak stress metric measured by multifactorial stress equation (MSE) is plotted as a function of optical frequency domain imaging pullback distance for 3 patients with plaque ruptures at the site of culprit thrombi. **(B1 to B3)** The optical frequency domain imaging cross sections show the corresponding 5 locations of peak stress metric. Images highlighted in red indicate the cross sections with the maximum peak stress. **(C1 to C3)** The culprit rupture sites with thrombi, which correspond to the locations of the asterisks in **(A1 to A3)**. The culprit rupture site was located adjacent to the location of the maximum peak stress metric.

Other biomechanical studies using FEM indicate a large variability in peak stress values (100 to 900 kPa) measured in ruptured and intact coronary plaques in patients (21–23). In this study, we observed peak stress values ranging from ~100 to 1,000 kPa even in nondisrupted plaques. These higher peak stress values may be attributed to a larger percentage of patients with ACS (40%) included in our study who had larger NC plaques with increased overall plaque burden. Thus, it is likely that plaques with complex geometries, irregular luminal boundaries, and heterogeneous subintimal structures resulted in greater stress concentrations. Furthermore, a majority of plaques in our study contained calcific nodules, which could amplify the measured peak stress up to 5-fold (20). The MSE approach described here will likely open critical opportunities for clinical investigations to determine the range of peak stress values in ACS versus stable angina patients.

In a separate pilot study conducted in 10 cadaveric hearts, we confirmed that composite OFDI-IVUS imaging improved the accuracy of quantifying plaque morphological parameters compared with the sole use of IVUS or OFDI (Supplemental Figure 1). This is because OFDI is superior to IVUS in detecting subsurface thin caps, microcalcifications, and minute irregularities with exquisite spatial resolution of ~10 μ m. However, the OFDI signal is rapidly attenuated in the NC obscuring the determination of the NC outer boundary. Conversely, IVUS provides a large imaging depth, albeit at reduced spatial resolution for measuring plaque outer boundaries. Consequently, we further showed that composite OFDI-IVUS determination of plaque geometry significantly improved the accuracy of estimating PSM compared with the sole OFDI or IVUS (Supplemental Figure 2, Supplemental Table 3).

In our study, FEM was used purely for the purpose of obtaining reference peak stress values and to derive the MSE (Equation 1). We further compared MSE-calculated PSM with the FEM-derived peak stress in 61 nonruptured NCFAs. The excellent correlation with high concordance and low measurement bias between the 2 approaches (Figure 5) shows that MSE can be used interchangeably with FEM. Thus, in practice, in a subset of 3 patients with ruptured NCFAs (Figure 6), through straightforward MSE measurements, we observed that peak stress was significantly elevated in the vicinity of the rupture site. Although further validation through prospective clinical testing is warranted, this initial result is significant because it indicates that just 6 morphometric measurements of plaque geometry may accurately localize rupture-prone sites.

STUDY LIMITATIONS. In the patient cohort investigated in this study, ruptured plaques were observed in only 3 patients; therefore, the MSE was applied to identify rupture sites in only these patients. In 3 patients with plaque ruptures we observed that the maximum PSM was elevated close to the site of plaque rupture (Figure 6). Because of the presence of culprit thrombi in the field of view, which limited our ability to view subsurface plaque morphology, we were unable to calculate the PSM at the precise image frame of the rupture site obscured by thrombus. Therefore, it is likely that the PSM value measured at the rupture site with thrombus may have been different from the observed PSM value at the adjacent site without thrombus. Future prospective, longitudinal clinical studies will be necessary to determine conclusively the associations among peak stress, coronary plaque ruptures, and subsequent thrombosis. In this study, the most time-consuming post-processing step involved OFDI-IVUS image co-registration through identification of image landmarks (see the Methods section, earlier), which added additional processing time and complexity. Recently, bimodality imaging systems have been approved by the U.S. Food and Drug Administration and likely will be available soon for patient use to enable tandem OFDI-IVUS imaging through a single integrated catheter, which will further reduce procedure time, patients' risks, and post-processing complexities (24,25). Following image co-registration in our study, plaque segmentation and parameter calculation were performed in just 2 min, with an additional 5 s for the MSE calculation of PSM for composite image pair. The use of 2-dimensional FEM in this study did not take into account the longitudinal shape of tortuosity of the coronary wall and out-of-plane deformations that could influence stress distributions. This was because coronary catheterization in patients was performed in conjunction with single-plane angiography, thereby precluding the evaluation of 3-dimensional coronary vessel shape. In the future, the use of biplane angiography or CT angiography (CTA) may allow us to include these additional parameters into a further refined MSE model that includes longitudinal coronary geometry and tortuosity metrics. However, drawbacks of biplane angiography and CTA include the substantial increase in procedure time, contrast volume, radiation dose, and cost (26); therefore, these approaches may not be suitable for routine PCI procedures. Future studies in patients may likely allow us to investigate the comparative effectiveness of including 3-dimensional geometry metrics in predicting plaque rupture in patients and may help in identifying patient

subgroups that may benefit from the inclusion of biplane angiography or CTA.

CONCLUSIONS

We present a novel and straightforward approach to estimate peak stress in coronary plaques. With a simple analytical equation that defines the cumulative influence of 2-dimensional plaque geometry, we demonstrated that the PSM could be accurately estimated, which may potentially serve as a pivotal biomechanical indicator of plaque rupture risk in patients. Consequently, this new approach obviates the need for tedious and mathematically intensive FEM. In the future, we anticipate that the MSE could be used in conjunction with routine OFDI and IVUS evaluation, which will enable further investigation into the relationship between biomechanical stress profiling and subsequent plaque-related events.

ACKNOWLEDGMENTS The authors thank Dr. Hang Lee of the Harvard Catalyst Program for providing statistical consultation on data analysis, and Xuan Pei for her assistance with the ABAQUS software.

ADDRESS FOR CORRESPONDENCE: Dr. Seemantini K. Nadkarni, Wellman Center for Photomedicine, Massachusetts General Hospital, Harvard Medical School, 50 Blossom Street, Boston, Massachusetts 02114. E-mail: snadkarni@mgh.harvard.edu.

PERSPECTIVES

COMPETENCY IN MEDICAL KNOWLEDGE: Using a simple analytical solution that defines the cumulative influence of plaque geometry, the MSE obviates the need for mathematically-intensive FEM and provides an index of peak stress derived simply from 6 plaque parameters. Thus, the PSM may potentially serve as a pivotal biomechanical indicator of plaque rupture risk in patients.

TRANSLATIONAL OUTLOOK: The peak stress in the fibrous cap of NCFAs is a likely predictor of plaque rupture and major adverse cardiovascular events in patients. The use of MSE in conjunction with OFDI and IVUS imaging will enable future investigations to ascertain the relationships among biomechanical stress, plaque rupture, and acute coronary events. The use of MSE in conjunction with OFDI and IVUS evaluation will enable further investigation into the relationship between biomechanical stress profiling and subsequent acute coronary events. Additional studies, such as using dual-sensor OFDI-IVUS, are needed to investigate the use of biomechanical stress profiling for the prognostic evaluation of patients with atherosclerosis.

REFERENCES

1. Virmani R, Kolodgie FD, Burke AP, Farb A, Schwartz SM. Lessons from sudden coronary death: a comprehensive morphological classification scheme for atherosclerotic lesions. *Arterioscler Thromb Vasc Biol* 2000;20:1262-75.
2. Finn AV, Nakano M, Narula J, Kolodgie FD, Virmani R. Concept of vulnerable/unstable plaque. *Arterioscler Thromb Vasc Biol* 2010;30:1282-92.
3. Kubo T, Imanishi T, Takarada S, et al. Assessment of culprit lesion morphology in acute myocardial infarction: ability of optical coherence tomography compared with intravascular ultrasound and coronary angiography. *J Am Coll Cardiol* 2007;50:933-9.
4. Brugaletta S, Garcia-Garcia HM, Serruys PW, et al. NIRS and IVUS for characterization of atherosclerosis in patients undergoing coronary angiography. *J Am Coll Cardiol Img* 2011;4:647-55.
5. Cheruvu PK, Finn AV, Gardner C, et al. Frequency and distribution of thin-cap fibroatheroma and ruptured plaques in human coronary arteries: a pathologic study. *J Am Coll Cardiol* 2007;50:940-9.
6. Serruys PW, Garcia-Garcia HM, Regar E. From postmortem characterization to the in vivo detection of thin-capped fibroatheromas: the missing link toward percutaneous treatment: what if Diogenes would have found what he was looking for? *J Am Coll Cardiol* 2007;4:50:950-2.
7. Toutouzas K, Karanasos A, Tsiamis E, et al. New insights by optical coherence tomography into the differences and similarities of culprit ruptured plaque morphology in non-ST-elevation myocardial infarction and ST-elevation myocardial infarction. *Am Heart J* 2011;161:1192-9.
8. Loree HM, Kamm RD, Stringfellow RG, Lee RT. Effects of fibrous cap thickness on peak circumferential stress in model atherosclerotic vessels. *Circ Res* 1992;71:850-8.
9. Sangiorgi G, Taylor AJ, Farb A, et al. Histopathology of postpercutaneous transluminal coronary angioplasty remodeling in human coronary arteries. *Am Heart J* 1999;138:681-7.
10. Thondapu V, Bourantas CV, Foin N, Jang I-K, Serruys PW, Barlis P. Biomechanical stress in coronary atherosclerosis: emerging insights from computational modelling. *Eur Heart J* 2016;37:81-92.
11. Speelman L, Akyildiz A, Den Adel B, et al. Initial stress in biomechanical models of atherosclerotic plaques. *J Biomech* 2011;44:2376-82.
12. Ohayon J, Finet G, Gharib AM, et al. Necrotic core thickness and positive arterial remodeling index: emergent biomechanical factors for evaluating the risk of plaque rupture. *Am J Physiol Heart Circ Physiol* 2008;296:H717.
13. Brown AJ, Teng Z, Calvert PA, et al. Plaque structural stress estimations improve prediction of future major adverse cardiovascular events after intracoronary imaging. *Circ Cardiovasc Imaging* 2016;9:e004172.
14. Costopoulos C, Huang Y, Brown AJ, et al. Plaque rupture in coronary atherosclerosis is associated with increased plaque structural stress. *J Am Coll Cardiol Img* 2017;10:1472-83.
15. Ohayon J, Finet G, Treyve F, Rioufol G, Dubreuil O. A three-dimensional finite element analysis of stress distribution in a coronary atherosclerotic plaque: in-vivo prediction of plaque rupture location. In: Payan Y, editor. *Biomechanics Applied to Computer Assisted Surgery*. 37; 2005; p 225-41.
16. Goyal M, Kim SW, Mishra S, et al. Morphological characteristics of optical coherence tomography defined plaque fissure in patients with acute coronary syndrome. *Heart Vessels* 2019;34:427-34.

17. Villiger M, Otsuka K, Karanasos A, et al. Repeatability assessment of intravascular polarimetry in patients. *IEEE Trans Med Imaging* 2018;37:1618-25.
18. Narula J, Nakano M, Virmani R, et al. Histopathologic characteristics of atherosclerotic coronary disease and implications of the findings for the invasive and noninvasive detection of vulnerable plaques. *J Am Coll Cardiol* 2013;61:1041-51.
19. Finet G, Ohayon J, Rioufol G. Biomechanical interaction between cap thickness, lipid core composition and blood pressure in vulnerable coronary plaque: impact on stability or instability. *Coron Artery Dis* 2004;15:13-20.
20. Kelly-Arnold A, Maldonado N, Laudier D, Aikawa E, Cardoso L, Weinbaum S. Revised microcalcification hypothesis for fibrous cap rupture in human coronary arteries. *Proc Natl Acad Sci U S A* 2013;110:10741-6.
21. Holzapfel GA, Mulvihill JJ, Cunnane EM, Walsh MT. Computational approaches for analyzing the mechanics of atherosclerotic plaques: a review. *J Biomech* 2014;47:859-69.
22. Kok AM, Speelman L, Virmani R, Steen AF, Gijzen FJ, Wentzel JJ. Peak cap stress calculations in coronary atherosclerotic plaques with an incomplete necrotic core geometry. *Biomed Eng Online* 2016;15:48.
23. Cheng GC, Loree HM, Kamm RD, Fishbein MC, Lee RT. Distribution of circumferential stress in ruptured and stable atherosclerotic lesions. A structural analysis with histopathological correlation. *Circulation* 1993;87:1179-87.
24. Yin J, Li J, Chen Z, et al. Novel combined miniature optical coherence tomography ultrasound probe for in vivo intravascular imaging. *J Biomed Opt* 2011;16:060505.
25. Novasight Hybrid System Recives FDA 510(k) Clearance in 2018. Available at: <https://www.fdanews.com/articles/186646-novasight-hybrid-system-receives-fda-clearance>. Accessed on November 1, 2018.
26. Sadick V, Reed W, Collins L, Sadick N, Heard R, Robinson J. Impact of biplane versus single-plane imaging on radiation dose, contrast load and procedural time in coronary angioplasty. *Br J Radiol* 2010;83:379-94.

KEY WORDS atherosclerosis, biomechanics, computational modeling, finite element, plaque rupture, stress

APPENDIX For a supplemental materials and methods section, tables, and figures, please see the online version of this paper.